EMBRY-RIDDLE
Aeronautical University

Simulation and Analysis of 3D Optical Devices through the use of Additive Manufacturing

Graduate Research Project, WiDE Lab

Alora Mazarakis

Advisor: Dr. Eduardo Rojas-Nastrucci, Ph.D.,

May 5, 2021

Contents

Abstract –

The utilization of silicon photonics and integrated optics provide a transformative solution to many technological challenges presented today. The manufacturing and testing of these devices and their interconnects has historically been performed in a cleanroom environment using advanced semiconductor technologies, hence requiring costly infrastructure and an advanced workforce. Advances in additive manufacturing have yielded the two-photon polymerization method, among whose various intended applications is the fabrication of optical devices. In this work, through the use of the two-photon polymerization method and FDTD simulations, optical passive components are simulated and fabricated to demonstrate the capability of this effective new additive manufacturing method.

1. Introduction

Current optical systems based on discreet components require expensive and comprehensive manufacturing resources. The current process for the fabrication and integration of integrated optics devices requires the use of a clean room environment, skilled technicians that have been thoroughly trained in the process, many expensive pieces of equipment, and a long lead time. While optical component boast an extensive list of technological upgrades such as super high-speed communications and wide bandwidths, the integration of these components into large scale production processes is not time efficient nor cost-effective using these traditional processes. Due to recent advances is additive manufacturing technology, the capability to print these components rather than painstakingly develop them is now a possibility. The effectiveness of this 3D printing process using lasers and resin is currently being evaluated and could potentially alleviate a lot of the issues with the traditional fabrication process.

It this paper, additive manufacturing in addition to the design and simulation of photonic components, specifically optical waveguides, will be discussed and the limitations of this process will be presented.

2. Applications

While the optical waveguide geometries presented are common components utilized in many photonic networks, the designs to be discussed were designed for two applications in mind: the use of optics in wearable biosensing devices, and the effects of microgravity on additively manufactured optical components.

In order to create biosensing technology which allow for flexibility, wearability, ease of testing, and high-fidelity readings, 3D optical devices are able to be additively manufactured to meet these specifications. While 3D optical devices offer the necessary parameters to address this problem, fundamental research is still required to understand and simulate the methods that would be best utilized on this technology. The additive manufacturing process used to fabricate optical components involves micrometer level techniques that require complex modeling and test trials.

The additive manufacturing resin-based materials claim to provide a low-refractive index with rigid structural stability. The use of photonic and optical devices in space-based applications would require these same parameters to be successful in a micro-gravity operational environment. Through collaboration with space science partners, the geometries that will be further discussed are preliminary designs which represent a final configuration to be testing in the microgravity environment of the international space station.

3. Modelling and Tools

Two primary tools were utilized throughout the design and manufacturing process. All simulations were carried out using the Finite Difference time-domain method (FDTD) functionality of the Ansys Lumerical Software. This program is intended to be used in the modeling and parameter derivation of photonic devices and materials. Each component was modelling in FDTD, their outputs analyzed and modelled in 3D using Autodesk Inventor to prepare the components for manufacturing once the simulations produced the desired output.

The other primary tool used is the Nanoscribe Photonic Professional GT2 3D printer, for use in microfabrication. The Nanoscribe machine utilizes a two-photon polymerization method which produces filigree structures withing a resin material. This hardware provides ultra-precise printing, allowing for minimal error in the physical components during manufacturing. This also allows for complex structures such as lenses to be manufactured. The laser used to cure the resin structure is a focused, femtosecond-pulsed, near-infrared (NIR) laser. Once the component has been printed using the laser, it is gold-sputtered and inserted into the scanning electron microscope (SEM) for imaging.

3.2 Design

In lumerical, the CAD functionality allows design and dimensioning of components as well as the definition of inputs, simulation regions, monitors, and bandwidth. Each model was created using the IP-n162 material provided by nanoscribe for optical components (the specification of this material is discussed further in section 4) with an SiO_2 cladding (shown in wireframe). The dimensionality of each component was derived empirically, with dimensions being adjusted as necessary to derive a desired output. The three components designed are a 3db directional coupler, a 3db Y-branch splitter, and straight optical waveguide. Each component as designed in lumerical is shown in figure 1.

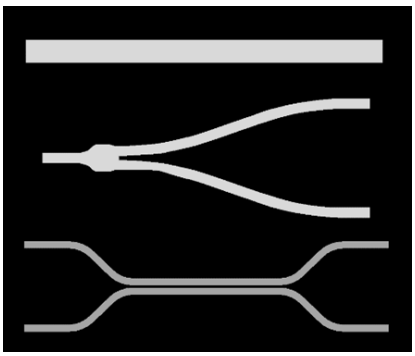

Figure 1. High level rendering of the (pictured from left to right) optical waveguide, Y-branch splitter, and directional coupler that were modelled and fabricated. (Not to size).

The Y-branch splitter was designed to allow for low combiner loss. As shown in Figure 2, a taper was added to the junction where $w_2 = 2w_1$ and θ = 2*arctan(h/l).

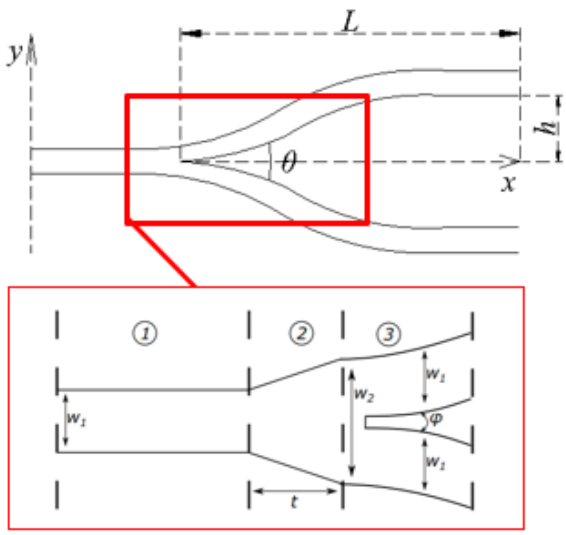

Figure 2: Dimensions of taper in splitter. [1]

This design improves the loss that occurs during the optical splitting, as well as re-combining should the component be used as a combiner. The resultant design can be seen in Figure 3.

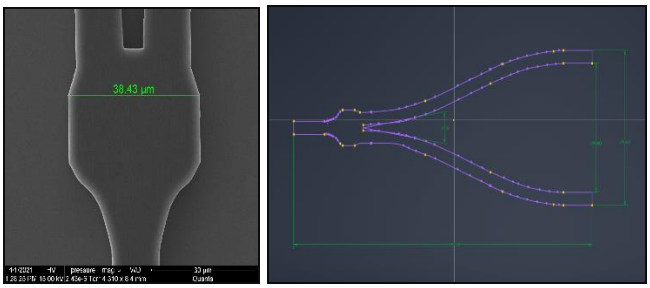

Figure 3: Preliminary design, dimensioning and manufacturing of splitter with taper.

The modelling coupler posed a particular challenge as the coupling factor is based on a ratio of the coupling length, lc, to the waveguide gap, gc. The directional coupler can be thought of from a design standpoint as two s-bend waveguides – the s bend, length, and width x height of the waveguides all contribute to their coupling factor as well as their effectiveness as an optical fiber.

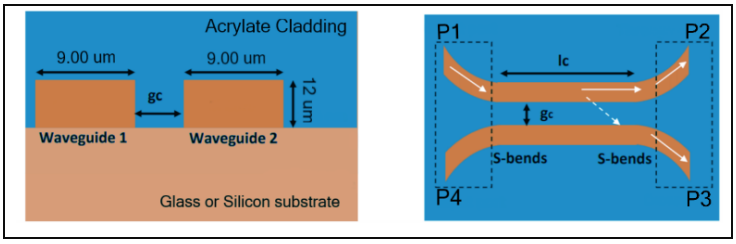

Figure 4. Critical coupler dimensions and the resulting values [2].

As this component was developed empirically as an alternative to a numerical derivation, various design iterations were simulated before a nominal output was achieved. Shown in Figure 5 is the progression of E radiation plots as the design was optimized based on dimensionality.

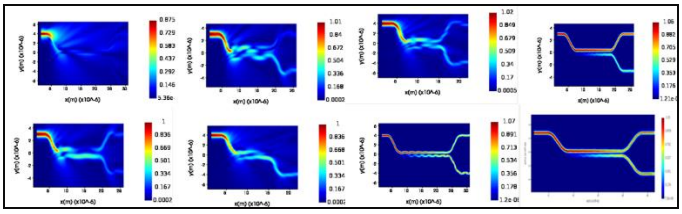

Figure 5: Progression of E radiation plot outputs through the design of a directional coupler.

In each iteration, the gap, g_c, was altered by 0.1 um proportional to a change in the width of each waveguide by 1 um and a change in the coupling length, l_c by 2um. The goal in this instance was to keep the proportionality of each component while sizing to an appropriate waveguide width to meet constraints on both the structural stability of the printing process as well as for use in the applications discussed in section 2.

4. Simulation and Analysis

At a high level, the FDTD method solves Maxwell's equations in the time domain to produce an output of both the magnetic (H) and electric (E) fields in space. In this implementation, the relevant performance metrics are the E-field radiation graph and the S-parameters. The components are intended for utilization at 1550 nm, therefore the components are designed to support single mode operation. Each component will be discussed individually in terms of their final performance.

4.1 Straight Optical Waveguide Performance

The straight optical waveguide was designed to be a 200um x 12um x 8um IP-n162 core with a urethane acrylate and acrylate monomer blend cladding. For the purpose of the simulation, the dimensions of the cladding are of no consequence as the simulation area is only defined around the core to save memory and simulation time. An isometric view of this design is shown in Figure 6.

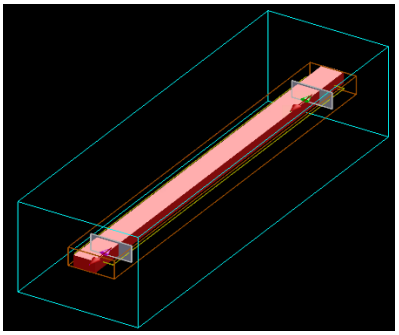

Figure 6: Lumerical rendering of straight optical waveguide within wireframe cladding.

The simulations were run at a center wavelength of 1.55 um (1550 nm) with a band of 0.5. The output E radiation plots for both an x-y plane view and a y-z plane view

cross sectional can be seen in Figure 7. This is indicative of a good single-mode propagation throughout the waveguide. The single center of radiation depicts a single-mode operation, as a multi-mode operation would have two or more radiation radii within the planar core of the structure.

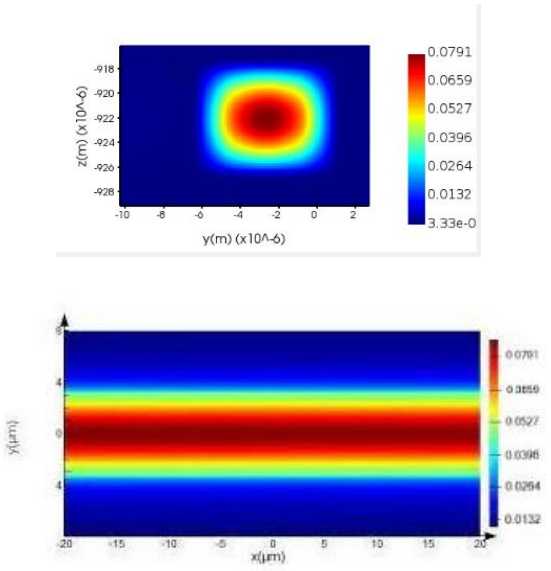

Figure 7: Cross-sectional y-z E-plot representation of straight optical waveguide (top) and x-y top view of E-plot for straight optical waveguide.

4.2 Y-branch Splitter Performance

Similar to that of the straight optical waveguide, the Y-branch splitter also yielded a favorable response in its E-radiation output plots. Shown in Figure 8 is the splitter with simulation region, ports, and a cladding represented. Its E-field output graphs are equivalently shown in Figure 9.

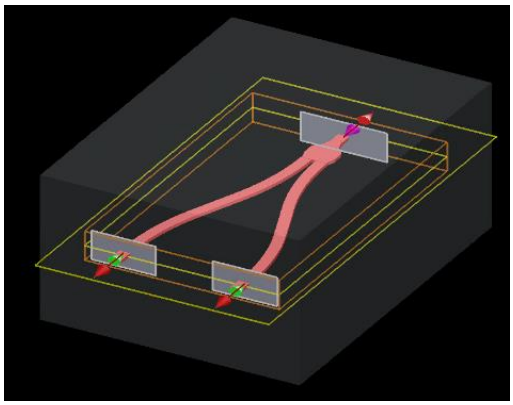

Figure 8: Isometric rendering of Y-branch splitter in Lumerical with cladding outer region.

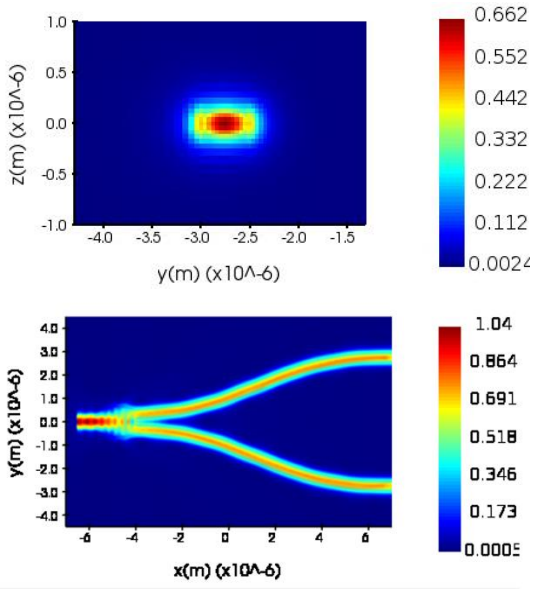

Figure 9: Cross-sectional y-z E-plot representation of splitter (top) and x-y top view of E-plot for splitter.

Because the design is symmetrical, a single E plot of either port will accurately represent both output ports. Here it can be seen that the cross-sectional area with no alternative modes developing elsewhere in the waveguide.

The S parameters for the splitter are shown in Figure 10. For the insertion loss, the main interest for this implementation are the TE curves. As shown, the curve's center peak is around 1.55, and therefore meets the design parameters.

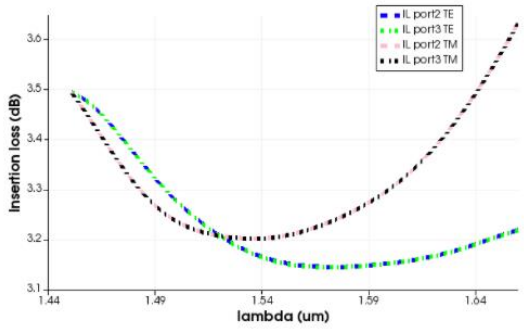

Figure 10: TE and TM insertion loss S-parameters for splitter.

4.3 2x2 Directional Coupler Performance

The lumerical CAD rendering is shown in Figure 11, the cladding is shown in wireframe format surrounding the geometry. The simulation was defined to run at a center wavelength of 1.55um

with a bandwidth of ±0.1. The output E-radiation plot of both the cross-sectional y-z view and the top-level x-y view are shown in _____.

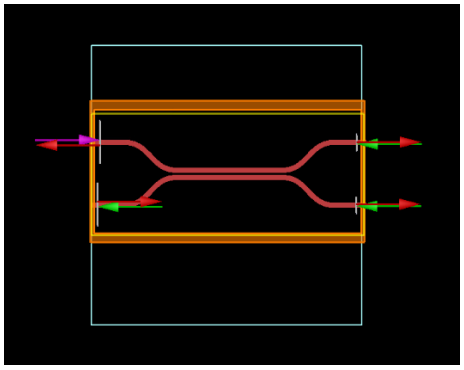

Figure 11: Rendering of directional coupler in lumerical with cladding wireframe.

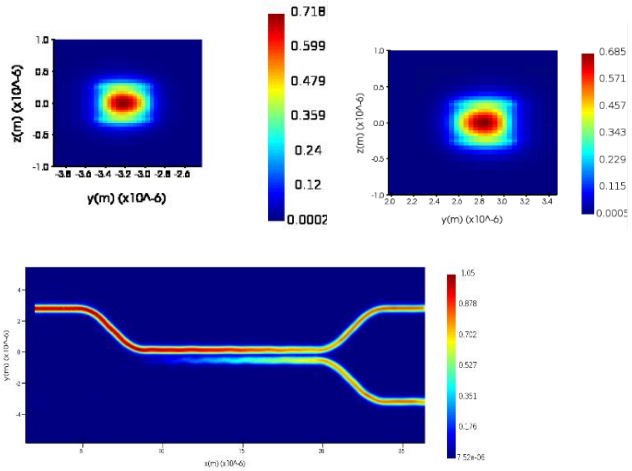

Figure 12: Cross-sectional y-z E-plot representation for output and coupled port of directional coupler (top) and x-y top view of E-plot for directional coupler.

While the coupler's geometry is also symmetrical, the coupling of the waveguides produces an output such that both ports should be analyzed separately, in addition to the S-parameters which are shown in Figure 13.

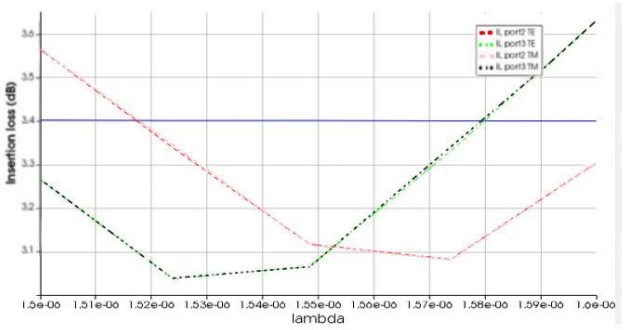

Figure 13: TE and TM insertion loss S-parameters for directional coupler.

Like the splitter, the primary interest in this plot are the TE plots, as the magnetic field is not being analyzed in this study. The plot's center for the TE lines are around 1.52 and 1.57 per port, respectively. This is near enough to the target center wavelength that it is appropriate to say that this geometry meets the design constraints.

5. Manufacturing

The completed and analyzed components were scaled proportionally to meet the size constraint of 10um minimum waveguide width are then prepared to be printed using the Nanoscribe GT2. The first step of this process is to recreate the geometries in a 3D CAD program. The program chosen for this study was Autodesk inventor, due to the ease of reproduction from a pre-existing drawing. Each component was drawn and extruded to the proportional dimensions corresponding with each simulation output. These Drawings can be seen in Figure 14.

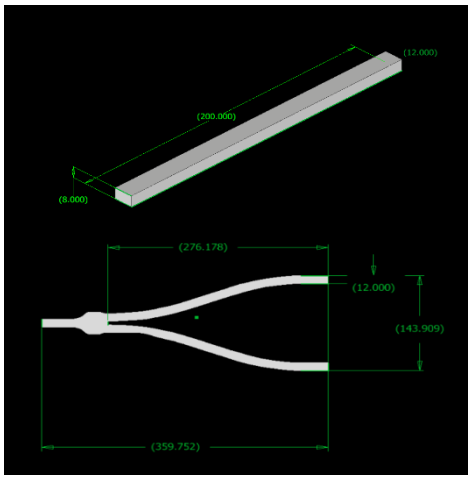

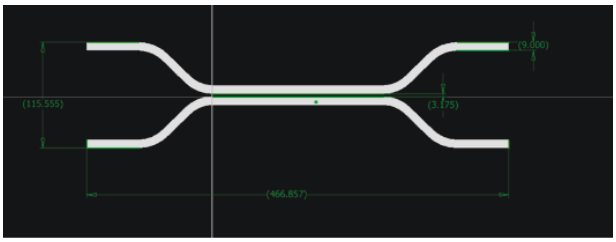

Figure 14: Three optical components with manufacturing final dimensions as modelled in AutoCAD inventor to be printed.

The drawings are converted to .stl and sent to Nanoscribe's 3D meshing GUI, DeScribe, where the patterns and printing paths are calculated and set. The final printing format is then sent to the Nanoscribe execution software, Nanowrite where the components are printed.

As previously described, the Nanoscribe GT2 uses a method called Two-Photon polymerization, where to focal point of a laser cures a resin material into a structure through individual pixel-like components called voxels. A visual description of this process is shown in Figure 15Figure 14.

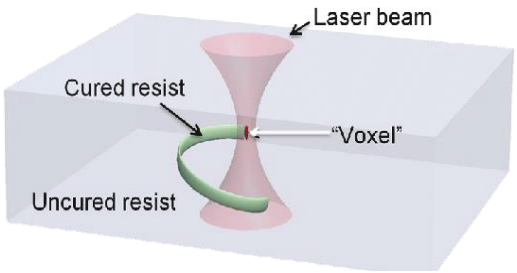

Figure 15: Simplified visualization of the two-photon polymerization process [3].

The finalized components are shown in Figure 16. Note that there is an error tolerance of ±7% when fabricating at this micro scale.

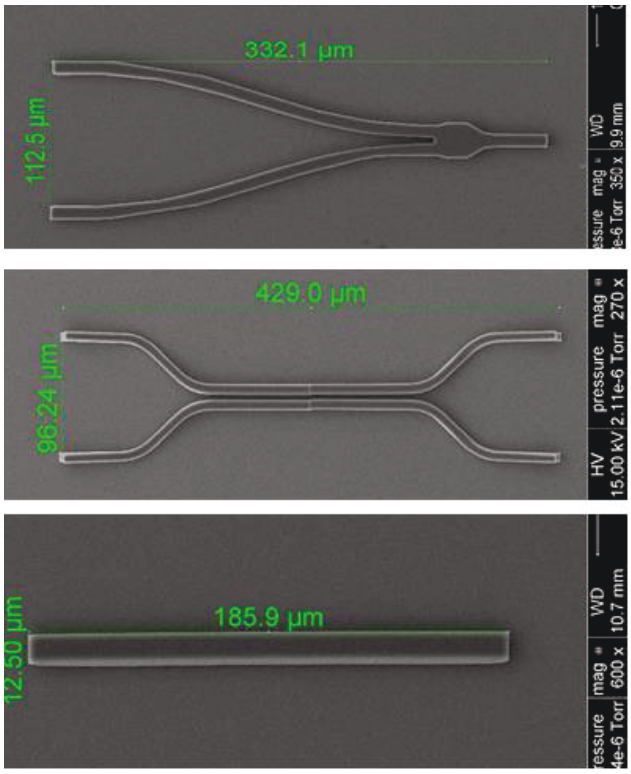

Figure 16: Three fabricated optical components from the Nanoscribe printer: Splitter (top), directional coupler (middle), straight optical waveguide (bottom).

5.2 Issues and Future Improvements

As this process is a fairly recent advancement, there are several imperfections in the physical components. One of the issues that arose during manufacturing was the sizing of the components with respect to the sizing capability of the Nanoscribe. The maximum single "block" of printing that can be accomplished by the machine is a radius of 400 um. Because the coupler design exceeded this size, a seam was to be placed somewhere along the component where the second "block" of cured resin pattern was placed. The choice was made to place this seam in the straight section of the component rather than in the S-bend, as the refraction in the bend is more sensitive to design inconsistencies than in a straight section. Even so, extensive research into the effects of these seams has yet to have been accomplished, so the true effects on the physical components are unknown. An example of this seam is shown in Figure 17.

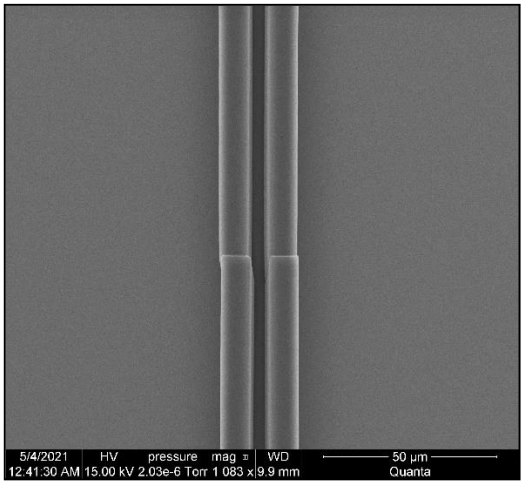

Figure 17: Seam between printing "blocks".

Another issue that was seen during manufacturing occurred after the components were coated in the sputtering machine. During the transition process between the sputtering machine to the SEM (a short distance, accomplished by trained personnel) some of the gold appeared to have been damaged or punctured in this same seam area. The causes of this anomaly are unknown, however it could potentially be attributed to the sharp difference in geometry where the seam is located, leading to instability in the gold coating. While this would not affect performance, as once the components are sputtered, they are no longer usable, it does affect the quality of the images that were able to be acquired from this process. An example of this "falling-out" anomaly can be seen in Figure 18.

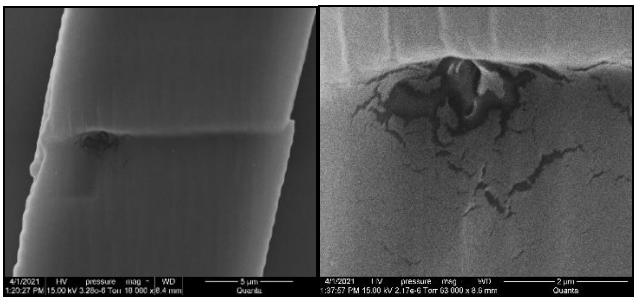

Figure 18: Gold sputtering "fall out".

Lastly, in future research the components should include a cured resin cladding. The components in this study did not include a cladding as this would make the core difficult to image and analyze. This process of adding a cladding would include coating the micro components with a very specific amount of the aliphatic urethane acrylate and acrylate monomer blend to be cured around the components through the use of a microscope.

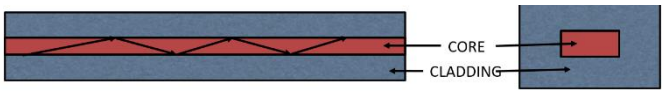

Figure 19: Cladding/Core relationship.

5.3 Future Designs

The resin material used for these components, IP-n162, has properties designed by nanoscribe specifically for use in micro-optics. Lenses are optimal components to be used for coupling light in and out of a fiber optic waveguide, so for the purpose of simulating the capability of the Nanoscribe machine, a prototype of such a fiber-lens component was designed and printed. This fiber-lens interface can be seen in Figure 20and involves the use of a Fresnel lens to disperse the light from the waveguide at its' port. This component was designed using scaffolding technique rather than the available optical component technique, but Nanoscribe as provided an example of what a singularly designed optical lens might look like. The challenge in creating a component such as this lies in the printing configuration, as once a component is printed onto a slide, it is near impossible to remove said component without causing significant structural damage.

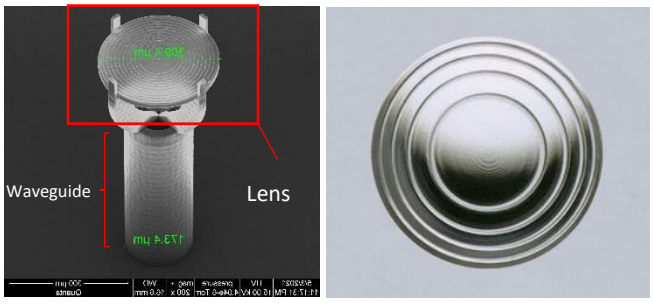

Figure 20: Optical fiber-lens interface prototype (left). Fresnel lens as demonstrated by Nanoscribe (right). [7]

6. Conclusion

Three basic optical components were modelled, simulated, and fabricated to demonstrate the capability of the two-photon polymerization additive manufacturing method. In addition to the components being successfully manufactured, the materials of the cladding and core of the optical components were all simulated and shown to be effective for use in components with these geometries. Various improvements to the manufacturing and imaging process were recommended, and a prototype of a potential interface structure was proposed. Based on the findings of this study, it was found that the two-photon polymerization method shows great potential as being an effective, time-efficient, and cost-efficient solution to the photonics manufacturing difficulties that are currently experienced throughout the micro-manufacturing industry.

7. Bibliography

[1] J. H. B. S. S. U. J. D. P. B. Andrew Katumba, "Low-Loss Photonic Resevoir Computing with Multimode Photonic Integrated Circuits," *Scienctific Reports,* p. 22, 2019.

[2] N. M. F. N. C. C. Erica C. Graham, "Silicon Photonic 2 X 2 Power Splitter with S-Bend Configuration," in *COMSOL Conference*, Boston, 2019.

[3] S. &. D. C. &. C. J. &. P. R. Saha, "Effect of Proximity of Features on the Damage Threshold During Submicron Additive Manufacturing Via Two-Photon Polymerization," *Journal of Micro and Nano-Manufacturing,* 2017.

[4] D. H. E. A. R.-N. T. M. W. V. R. B. Roger B. Tipton, "Laser Enhanced Direct Print Additive Manufacturing of Embedded Circular Cross-Section Optical Fiber Interconnects for Board Level Computing Devices”," 2020.

[5] S. C. a. B. K. D. “.-I. D. C. f. I. S. P. R. K. Gupta, "“Wavelength-Independent Directional Couplers for Integrated Silicon Photonics,”," J. Lightwave Technol., vol. 35, no. 22, pp. 4916–4923, 2017. .

[6] G. &. S. A. &. V. S. Singh, "Estimation of the performance of a 3-dB Y-junction optical coupler with a channel profile of proton-exchanged lithium niobate.," in *.Physics of Wave Phenomena*, 2013.

[7] "IP-n162 resin for micro-optics," Nanoscribe, 2021. [Online]. Available: https://www.nanoscribe.com/en/products/ip-resins/ip-n162.

[8] D. Z. M. K. Z. Muddassir Iqbal, "Designing Optical Waveguides: Myth and Reality," *Brazilian Journal of Physics,* p. 17, 2020.

[9] C. L. K. P. M. RICCARDOMARCHETTI, "Coupling strategies for silicon photonicsintegrated chips," *Photonics Research,* vol. 7, no. 2, 2019.

With special thanks to Ansys Lumerical discussion board